Received: 1 July 2023 | Revised: 21 December 2023 | Accepted: 24 January 2024

DOI: 10.1002/nbm.5123

RESEARCH ARTICLE

NMR IN BIOMEDICINE WILEY

Interleaved trinuclear MRS for single-session investigation of carbohydrate and lipid metabolism in human liver at 7T

Simone Poli[1,2,3] | Ahmed F. Emara[4] | Naomi F. Lange[5,6] | Edona Ballabani[4] | Angeline Buser[4] | Michele Schiavon[7] | David Herzig[4] | Chiara Dalla Man[7] | Lia Bally[4] | Roland Kreis[1,2]

[1]MR Methodology, Department for Diagnostic and Interventional Neuroradiology, University of Bern, Bern, Switzerland

[2]Translational Imaging Center (TIC), Swiss Institute for Translational and Entrepreneurial Medicine, Bern, Switzerland

[3]Graduate School for Cellular and Biomedical Sciences, University of Bern, Bern, Switzerland

[4]Department of Diabetes, Endocrinology, Nutritional Medicine and Metabolism UDEM, University Hospital Bern, Bern, Switzerland

[5]Department of Visceral Surgery and Medicine, Inselspital, Bern University Hospital, University of Bern, Bern, Switzerland

[6]Graduate School for Health Sciences, University of Bern, Bern, Switzerland

[7]Department of Information Engineering (DEI), University of Padova, Padua, Italy

Correspondence
Roland Kreis, MR Methodology, University Bern, Freiburgstr. 3, CH-3010 Bern, Switzerland.
Email: roland.kreis@insel.ch

Funding information
Swiss National Science Foundation, Grant/Award Number: PCEGP3_186978; Diabetes Center Bern

Abstract

The liver plays a central role in metabolic homeostasis, as exemplified by a variety of clinical disorders with hepatic and systemic metabolic disarrays. Of particular interest are the complex interactions between lipid and carbohydrate metabolism in highly prevalent conditions such as obesity, diabetes, and fatty liver disease. Limited accessibility and the need for invasive procedures challenge direct investigations in humans. Hence, noninvasive dynamic evaluations of glycolytic flux and steady-state assessments of lipid levels and composition are crucial for basic understanding and may open new avenues toward novel therapeutic targets. Here, three different MR spectroscopy (MRS) techniques that have been combined in a single interleaved examination in a 7T MR scanner are evaluated. ^{1}H-MRS and ^{13}C-MRS probe endogenous metabolites, while deuterium metabolic imaging (DMI) relies on administration of deuterated tracers, currently ^{2}H-labelled glucose, to map the spatial and temporal evolution of their metabolic fate. All three techniques have been optimized for a robust single-session clinical investigation and applied in a preliminary study of healthy subjects. The use of a triple-channel ^{1}H/^{2}H/^{13}C RF coil enables interleaved examinations with no need for repositioning. Short-echo-time STEAM spectroscopy provides well resolved spectra to quantify lipid content and composition. The relative benefits of using water saturation versus metabolite cycling and types of respiratory synchronization were evaluated. ^{2}H-MR spectroscopic imaging allowed for registration of time- and space-resolved glucose levels following oral ingestion of ^{2}H-glucose, while natural abundance ^{13}C-MRS of glycogen provides a dynamic measure of hepatic glucose storage. For DMI and ^{13}C-MRS, the measurement precision of the method was estimated to be about 0.2 and about 16 mM, respectively, for 5 min

Abbreviations: AHP, adiabatic hyperbolic-secant pulse; BH, breath-holding; BMI, body mass index; CMRR, Center for Magnetic Resonance Research of the University of Minnesota; D-Glc, deuterated glucose; DMI, deuterium metabolic imaging; FWHM, full-width at half-maximum; GPC, glycerophosphocholine; HDO, deuterated water; HLC, hepatocellular lipid content; MC, metabolite cycling; MCL, mean chain length; ndb, number of double bonds; NOE, nuclear Overhauser enhancement; nPU/FA, number of polyunsaturated bonds/fatty-acyl chain; nPU/UFA, number of polyunsaturated bonds per unsaturated fatty-acyl chain; nUFA, number of unsaturated fatty-acyl chains; OVS, outer-volume suppression; PCho, phosphocholine; RS, respiratory synchronization; SAR, specific absorption rate; SI, saturation index; SNR, signal-to-noise ratio; STEAM, stimulated echo acquisition mode; T_E, echo time; TMA, trimethylammonium; T_R, repetition time; VAPOR, variable pulse power and optimized relaxation delays; WS, water suppression.

Lia Bally and Roland Kreis contributed equally to this work.

scanning periods. Excellent results were shown for the determination of dynamic uptake of glucose with DMI and lipid profiles with ^{1}H-MRS, while the determination of changes in glycogen levels by ^{13}C-MRS is also feasible but somewhat more limited by signal-to-noise ratio.

KEYWORDS
carbohydrate metabolism, deuterium metabolic imaging, glucose, glycogen, lipid composition, liver metabolism

INTRODUCTION

The liver plays a central role in metabolic homeostasis and is a major site for synthesis, storage, and redistribution of carbohydrates and lipids. As a consequence, altered hepatic carbohydrate and lipid metabolism is indicative of a broad spectrum of metabolic diseases such as obesity, diabetes, and fatty liver disease. Disorders of hepatic metabolism can also lead to intrahepatic lipid accumulation and impaired glucose tolerance, which are key features of insulin resistance.[1–4]

Due to limited accessibility or need for invasive procedures, metabolic imaging is a promising method for in vivo investigations of liver metabolism in humans, in particular the dynamic monitoring of intrahepatic lipids, hepatic glucose and its storage in the form of glycogen. In this context, MRI and MRS[5–7] using proton, carbon, and deuterium MRS are ideally suited. To maximize convenience and overcome the challenge of reproducing metabolic situations (e.g., influence of nutrition and activity), investigations of lipid and glucose metabolism are ideally integrated within a single-session examination. Herein, we provide an overview of technical aspects characterizing three different MRS techniques (^{1}H-MRS, ^{13}C-MRS, and deuterium metabolic imaging, DMI), which offer dynamic and combined insights into hepatic glucose and lipid metabolism and were evaluated in this work.

^{1}H-MR. Single-voxel ^{1}H-MRS has become the gold standard for noninvasive quantification of hepatic lipid content, covering the whole range from very low lipid content encountered in young lean healthy subjects all the way to full-blown hepatic steatosis, while Dixon-type MRI is most useful for the pathologic range of lipid content.[8] ^{1}H-MRS is also especially useful for determination of lipid composition.[5] Hepatic lipid content exhibits a significant correlation with insulin resistance in vivo, which serves as the best predictor for the development of Type 2 diabetes (T2DM) and is a hallmark of metabolic dysfunction-associated fatty liver disease (MAFLD) or nonalcoholic fatty liver disease (NAFLD).[9] Hepatic lipid content quantification with ^{1}H-MRS thus provides data that closely correlate with biochemical and histologic hepatic lipid storage analysis and has therefore unparalleled sensitivity.[10,11]

Besides the multiple lipid resonances, hepatic in vivo MR spectra have been described to consistently feature only a metabolite peak at 3.2 ppm attributable to the trimethylammonium (TMA) peak of cholines and betaine, while the signals between 3.3 and 4 ppm have multiple origins - of interest, some of it was reported to substantially represent glycogen.[12,13]

Two alternative proton-based metabolic imaging modalities, not for lipid, but for glucose and glycogen monitoring, are known as glycoCEST[14] and glycoNOE.[15] These techniques rely on indirect detection of glucose and glycogen through magnetization exchange between the carbohydrates and water. While yielding higher signal-to-noise ratio (SNR) than does direct spectroscopy, glycoCEST and glycoNOE suffer from other technical issues, in particular the signal overlap with the direct saturation water peak, motion, and high energy deposition. In addition, the interpretation of the signals is challenged by its origin from both intracellular and extracellular compartments.[16]

For single-voxel ^{1}H-MRS, multiple aspects of the acquisition conditions are relevant and have been investigated for this study. (1) Transverse relaxation times are in general short for liver tissue. Therefore, STEAM with very short T_E was preferred over Hahn-echo-based methods with longer minimal echo times. (2) Respiratory motion compensation is crucial. Acquisitions are usually performed using either breath-holds, respiration triggering (by MR-navigator or external monitoring), or rhythmic breathing in sync with the MR sequence.[17] Two of them were evaluated. (3) Metabolite cycling (MC)[17–19] has been proposed for water signal elimination with the potential to track and mitigate residual phase and frequency shifts/drifts. Its benefit was tested. (4) Hepatic ^{1}H-MRS can be performed well at clinical field strengths of 1.5 or 3 T, but to obtain better spectral resolution for the separation of different lipid and metabolite peaks, ultra-high-field MRS was used here in accordance with earlier proposals.[17,20,21]

^{13}C-MRS. An established method for the quantification of storage and utilization of glycogen and lipids in liver is natural abundance ^{13}C-MRS.[9,22–24] It has advanced our understanding of alterations in postprandial hepatic metabolism in type 2 diabetes.[25,26] When using exogenous instead of naturally abundant ^{13}C substrates, MRS allows for more detailed metabolic insights such as the endocrine regulation of hepatic glycogen metabolism by insulin and glucagon,[27] including delineation of metabolic fluxes for development of metabolic models.[28,29] Its use in clinical research has been limited due to low sensitivity, long acquisition times, limitation to the analysis of large volumes, and high costs for ^{13}C-labelled substrates. When using ^{13}C-MRS, proton decoupling as well as nuclear Overhauser enhancement (NOE) is often performed to enhance SNR. Here, we propose to use it at 7T without decoupling.

^{2}H-MR. DMI is a spectroscopic technique based on ^{2}H-labelled tracers that has recently gained a lot of attention for use in humans.[30] Its effectiveness relies on the fact that ^{2}H is a nonradioactive isotope with low natural abundance, with a tissue concentration of about 10 mM mono-deuterated water only. Hence, not much background signal is present, but the natural abundance water signal can still be used as internal reference. With its favorable spin quantum number of 1 and short (but not ultrashort) relaxation times, DMI features higher sensitivity than ^{13}C-MRS for observation of labelled substrates and their downstream metabolites—but is inferior in terms of spectral resolution. DMI has primarily been developed as a tool to investigate tumor metabolism (mainly brain and liver) in animals[31] and humans,[32,33] but is increasingly being used for other metabolic indications.[6] For example, recent works showed the potential of DMI in measuring deuterated glucose (D-Glc) glycolytic flux,[34] brown adipose tissue in rats,[35] and underlying metabolic pathways.[36] The benefit of performing DMI at ultra-high magnetic field has been proven[37] and is further evaluated in this study. Most crucial for hepatic studies, it has also been shown that deuterated glycogen is not realistically detectable in vivo with DMI,[38] underscoring the necessity for complementary ^{13}C-MRS for its quantification—unless glycoNOE, glycoCEST, or the claim of Ouwerkerk et al.[12] that hepatic glycogen can be quantified with standard localized ^{1}H-MRS turn out to be robust methods as well.

Ideally, the investigation of hepatic lipid and carbohydrate metabolism using the above outlined techniques are performed in a single examination using an interleaved measuring protocol. Single-session assessments increase convenience, obviate the need for repositioning of the subject, and overcome the challenge of reproducing identical metabolic conditions (e.g., effect of diet and exercise). Here, we describe a setup for anatomic MRI of the liver, interleaved observation of hepatic dynamic uptake of glucose, its conversion into glycogen, and the evaluation of lipid content and lipid composition. It comprises a triple-tuned RF coil, a 7T MR system, and optimized MRS methods given the constraints of limited energy deposition and robustness of the examination. This work builds the foundation for future clinical applications, in particular the exploration of hepatic glucose and lipid metabolism in clinical phenotypes with known alterations.[39]

METHODS

Study population and study procedures

Examinations were performed within the framework of research studies that had been approved by the Ethics Committee Bern and all participants provided written informed consent before undergoing study-specific procedures.

- For MR protocol definition and parameter optimization for ^{13}C and ^{2}H-MRS 10 healthy subjects were investigated (4 males and 6 females, age 32.9 ± 8.9 years, body mass index (BMI) 24.3 ± 3.7 kg/m^{2}), of whom 8 were examined in an overnight fasted state.
- Dynamic interleaved ^{13}C-MRS and DMI data were obtained from an additional five healthy subjects (2 males and 3 females, age 40.9 ± 11.9 years, BMI 26.3 ± 4.2 kg/m^{2}) who adhered to a standardized eucaloric diet consisting of 40% carbohydrates for 48 h prior to the examination and were examined in an overnight fasted state.
- Hepatic ^{1}H-MRS data were obtained from six healthy subjects (5 males and 1 female, age 35.8 ± 8.7 years, BMI 24.2 ± 2.8 kg/m^{2}) with no dietary restrictions.

Doubly deuterated glucose ([6,6'-$^{2}H_2$]-glucose) was purchased from Euriso-Top, Cambridge Isotope Laboratories, Saint-Aubin, France. Following the recommendation of De Feyter et al.,[32] [6,6'-$^{2}H_2$]-Glc was preferred over singly deuterated [1-^{2}H]-Glc for the double content of deuterium nuclei and over perdeuterated [1,2,3,4,5,6,6′,-$^{2}H_7$]-Glc due to lower costs and ease of interpretation.

The volunteers had an oral intake of 60 g of [6,6'-$^{2}H_2$]-Glc, dissolved in tap water to reach a volume of 200 mL. The diluted solution was prepared in 50mL sized syringes, and an elongation tube attached to the syringe was utilized for the administration of the solution, following a baseline scanning period. This facilitated the intake while lying inside the MR scanner and avoiding potential displacement of the coil and change of position after baseline assessment.

MR system and phantoms

Data acquisition was performed on a 7T MR scanner (Terra, Siemens, Erlangen, Germany) using a ^{1}H/^{2}H/^{13}C triple-tuned transmit/receive surface coil (RAPID Biomedical, Rimpar, Germany). The coil was designed with a linearly driven loop for ^{2}H (diameter 16 cm) and ^{13}C (diameter 14 cm) combined with a quadrature-driven dual loop for ^{1}H (22 × 16 cm, if stretched on a flat surface). The coil housing allows for three unshielded reference phantom containers (diameter 25 mm, length 20 mm). To illustrate the coil performance, experimentally determined B_1 maps for ^{1}H and ^{13}C are provided in Supporting Information. For ^{1}H-MR (Figure S1), a standard flip-angle mapping sequence of the manufacturer was used with the coil loaded by a body coil phantom of adapted permittivity and permeability (14 L, roughly body-shaped phantom composed of polyvinylpyrrolidone, NaCl, and Germaben dissolved in water). Driven in quadrature mode, the flip-angle distribution was recorded for a driving

voltage such that a 90° pulse was reached in the center of the coil at approximately 2 cm from the coil surface. For ^{13}C (Figure S2), B_1^+ and B_1^- maps were obtained from hard-pulse MRSI scans recorded with varying pulse power from a NaCl-loaded, gadolinium contrast agent-doped water/ethanol phantom, where the fitted sine behavior of the MR signal as function of the driving voltage was converted to excitation field strength in microtesla and receive-field maps in arbitrary units. The excitation and receive profiles for the two heteronuclei are expected to be similar, given the almost identical coil geometries and wavelengths well below the dimensions of the human body for both cases. B_1^+ and coil sensitivity maps as measured for ^{13}C represent the expected surface coil profile with sensitive areas reaching at least half of the coil diameter into the object of study, while the B_1 profile for protons is somewhat more inhomogeneous.

An acetone solution, doped with 0.4 g of chromium and 0.08 mL of deuterated acetone, was produced as an external reference to correct for coil loading effects. The 8 mL cylindrical vial was inserted in the central cavity in the center of the $^2H/^{13}C$ loops in the back of the coil. A glycogen phantom consisting of a 2L cylindrical bottle was used to optimize ^{13}C and ^2H acquisitions. It was filled with glycogen Type II from oyster (100 mM) dissolved in distilled water (phosphate-buffered to pH 7.0, stored in the fridge at ~2°C). A 7cm spherical deuterated glucose phantom was also used to optimize ^2H acquisitions. It contained 25 mM [6,6'-$^2H_2$]-glucose, 25 mM undeuterated glucose, 5 mM deuterated and undeuterated acetone, and 1 mM sodium azide in a phosphate buffer at a pH 7.0.

Coil placement and MRI

Coil placement was performed with the subjects in supine position, referencing the liver with the iliac spine. The distance between coil center and jugular fossa was documented for potential repositioning.

Gradient-echo multiplane localizers (coronal, transversal, sagittal, and oblique directions, $T_R/T_E = 7.7/3.67$ ms, flip angle = 20°, resolution = 0.5 × 0.5 × 0.5 mm^3, slice thickness = 5 mm) were acquired for coil-placement verification and spatial reference with and without breath-holding (BH). If the examination involved [6,6'-$^2H_2$]-glucose ingestion another set of images was acquired after the intake and again at the end of the scan. A 2D B_1 map (2D gradient echo, $T_R/T_E = 6250/1.72$ ms, resolution = 4.0 × 4.0 × 4.0 mm^3) was acquired during a BH in the exhaled state (acquisition time = 14.0 s) for ^1H B_1^+ calibration.

MR sequences and their parameters in the clinical evaluation studies

^1H-MRS

Two STEAM sequences were used, one featuring ultrashort-echo time (6 ms) and VAPOR water suppression (WS) as obtained from the Center for Magnetic Resonance Research of the University of Minnesota (CMRR),[40] and an in-house sequence based on the vendor's product sequence with minimum T_E of 14 ms and MC instead of water saturation.[41] A VOI of 26 × 18 × 18 mm^3 was selected in the liver on the right side close to the surface coil but evading large blood vessels. VAPOR water-suppressed scans were acquired using respiratory synchronization (RS) with voluntary rhythmic breathing by the volunteer and $T_E = 6$ and 14 ms ($T_M = 30$ ms). Metabolite-cycled spectra were recorded in BH ($T_R = 1300$ ms, 12 acquisitions) and under RS with $T_E = 14$ ms ($T_M = 11$ ms). For RS, T_R was set according to the subject's preference between 4.0 and 5.5 s, resulting in a total acquisition time of 2 min 20 s–3 min 2 s. Spectral width was 5000 Hz and 2048 data points were acquired for all cases.

^{13}C-MRS

Final pulse-and-acquire spectra were recorded with adiabatic excitation (adiabatic hyperbolic-secant pulse, AHP, of 2 ms length, frequency centered on glycogen-C1 or acetone-C1) and minimal acquisition delay (150 μs) (40 000 Hz spectral width, 1024 data points; T_R 600 ms, 512 acquisitions, and total acquisition time 5 min 8 s for glycogen and T_R 500 ms, 500 acquisitions, and total acquisition time 5 min 1 s for the external standard). NOE polarization transfer was induced for glycogen scans only (fixed voltage set at 12 V, duration of 510 ms before excitation). No outer-volume suppression (OVS) and no ^1H-decoupling was used.

DMI

Final metabolite maps were recorded with conventional 3D-MRSI using a 0.50 ms rectangular excitation pulse (frequency centered on deuterated water, HDO; T_R 500 ms; four acquisitions with elliptical acquisition-weighting; 12 × 12 × 8 (right–left/anterior–posterior/inferior–superior)

phase encodings; nominal resolution of 18.3 × 18.3 × 27.5 mm^3; 1000 Hz spectral width and 512 data points; total acquisition time of 4 min 9 s). Placement and angulation of the MRSI grid made use of the reference markers within the coil housing.

MR sequence parameter optimization

^{1}H-MRS

The benefits from using short or ultrashort echo times (balancing signal loss for lipids with fast decrease of dominant water signal), different WS techniques (VAPOR or MC: benefit of strong reference signal in each shot versus worse overall WS performance), and different respiratory schemes (BH versus RS: routine feasibility of either scheme) were evaluated.

^{13}C-MRS

In vitro and in vivo experiments were performed to optimize excitation pulse length and amplitude, NOE power, and repetition time for maximum achievable signal efficiency as well as to judge the benefits from OVS regarding suppression of superficial myocellular glycogen signals. In vitro, the adiabatic pulse length was varied from 1 to 3 ms. At a fixed AHP length of 2 ms, the reference voltage for the AHP was varied from 0 to 366 V, the NOE voltage from 1 to 12 V, and T_R from 400 to 1500 ms—in acquisitions both without NOE and with NOE at maximum voltage (minimum attainable T_R of 600 ms due to specific absorption rate (SAR) limitations).

In vivo, the AHP length was varied from 1 to 2.5 s and comparisons were made between the cases without NOE, with NOE at 8.5 V, and with NOE at maximum voltage. T_R was varied from 450 to 750 ms, both with and without NOE, as well as with and without OVS on muscle and liver.

^{2}H-MRSI

Excitation pulse length, pulse type, and pulse voltage, as well as the spatial dependence of signal amplitude for different pulse types and voltages, were evaluated on D-Glc and HDO both in vitro and in vivo to find best acquisition parameters with regards to SNR and robustness of acquisition conditions for repeated scans. In vitro, pulse lengths were optimized on HDO, and pulse type was varied (AHP length ranged from 1 to 2.5 ms, rectangular excitation pulse length from 0.2 to 2 ms). AHP and rectangular pulse reference voltage varied from 50 to 366 V. The dependence of the MR signal on the distance from the coil was compared between rectangular and adiabatic excitation at different pulse voltages. In vivo, rectangular excitation pulse length was varied from 0.2 to 2 ms and reference voltage was varied from 5 to 300 V and reported for multiple distances from the coil. The dependence of the MR signal on the distance from the coil was compared between rectangular (pulse length = 0.5 ms, pulse voltage = 300 V) and adiabatic excitation (pulse length = 2.5 ms, pulse voltage = 343 V). Repetition time was evaluated on D-Glc and HDO in vivo on three subjects: D-Glc and HDO signals are reported as functions of T_R variation between 160 and 1000 ms.

Data processing and statistics

JMRUI[42] was used to post-process all spectra, including HLSVD[43] to filter out spectral components. AMARES[44] or FitAID[45] were used to fit the spectra.

For ^{1}H-MRS, data were aligned and phased using the water signal in the case of MC spectra, using the methylene lipid signal otherwise. Spectra were corrected for eddy currents. ^{1}H spectra were fitted with FiTAID using simulated metabolite base spectra for choline, phosphocholine (PCho), glycerophosphocholine (GPC), betaine, Glc, myo-inositol, and a representation for glycogen, which either consisted of a basis spectrum derived from a measured glycogen phantom (corrected for spectral contributions from free glucose, present in the solution) or of two broad Voigt lines at 3.7–3.8 ppm (one with 500 Hz Lorentzian and Gaussian widths, the other with 80 Hz Lorentzian and 200 Hz Gaussian widths) to model the spectral range between 3.1 and 4.2 ppm. Frequency offsets were fixed between metabolites and between the components of the lipid spectrum but allowed to vary against each other. Equivalent choice of prior knowledge was established for the Gauss width, while the zero-order phase was assumed to be identical for all components and Lorentzian widths (T_2) were taken from literature and kept fixed. The lipid resonances were modeled by eight Voigt lines describing the seven lipid entities labeled in Figure 1A with a broad "baseline" component (200 Hz Gaussian and 150 Hz Lorentzian widths) to better model the methylene proton peak at 1.3 ppm that did not fit well with only two narrow lines for the general methylene and the beta carboxyl methylene protons.

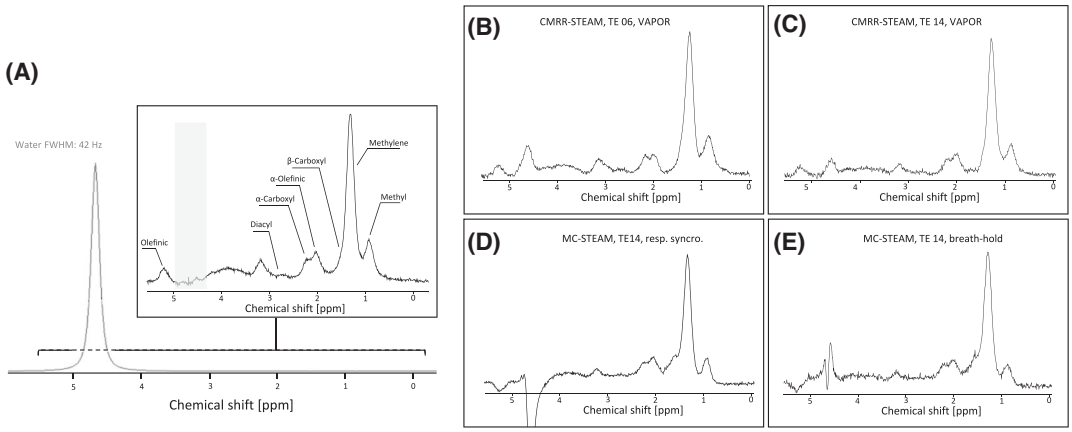

FIGURE 1 Representative hepatic in vivo ^{1}H-MR spectra from a healthy subject using different sequences, WS techniques, respiratory motion compensation, and echo times (T_E). A, Illustration of the spectra before and after WS, with labelled lipid components. B–E, Juxtaposed spectra obtained under different conditions. B versus C illustrates the effect of echo time (6 versus 14 ms) with all other parameters equal (CMRR-STEAM sequence, VAPOR WS, RS and 32 repetitions). C versus D compares VAPOR WS with MC water elimination at 14 ms T_E and also the CMRR sequence with a local in-house STEAM sequence. D versus E exposes potential differences based on RS, that is, RS versus breath-hold, where the latter uses fewer acquisitions and shorter T_R. The volunteer had a BMI of 21.2 kg/m^2 and a quantified HLC of 1.4%.

For ^{13}C-MRS, the spectra were post-processed and fitted as follows: HLSVD filtering was used to largely remove all lipid peaks, and spectra were zero-order phase corrected manually. The glycogen signal was fitted in FitAID as a doublet with equal amplitudes, identical phases, and a fixed frequency splitting of 164 Hz. Each doublet was fitted as sum of a narrow and a broad resonance with identical frequencies and with Lorentzian widths of 36 and 175 Hz, respectively, while the Gaussian width was limited to 0–150 Hz.

For DMI, six central voxels with respect to the center of the coil were manually preselected for maximum signal and their signals averaged. Voxels with potential substantial partial volume effect with nearby tissues were not considered. Each spectrum was zero-order phase corrected and quality checked from the water signal. Fitting was performed using two single Lorentzian lines (HDO at 4.7 ppm and D-Glc at 3.6 ppm) in AMARES. For HDO, amplitude, relative phase, and frequency were estimated, and linewidth restricted with a soft constraint (0–40 Hz). For D-Glc, the amplitude was estimated, the phase and frequency referred with a fixed shift to the values of HDO, and the linewidth restricted by a soft constraint (0–40 Hz). The first point of the free induction decays was truncated, and the first-order phase fixed to 0.15 ms (as empirically estimated).

Statistical analyses were performed in MATLAB and Microsoft Excel. Effects were considered statistically significant for $p < 0.05$ (exploratory effects, no correction for multiple tests).

Quantification

^{1}H-MRS

^{1}H-MRS lipid data were corrected for T_1 and T_2 relaxation times using literature values.[20,21] Hepatocellular lipid content (HLC) was estimated,[46] with the lipid spectrum composed of the following proton groups: olefinic (5.31 ppm), bisallylic (2.77 ppm), α-carboxylic (2.24 ppm), α-olefinic (2.02 ppm), β-carboxylic (1.6 ppm), methylene (1.30 ppm), and methyl (0.90 ppm). For lipid characterization, the following indices were estimated using definitions from previous work[46]: saturation index (SI), number of double bonds (ndb), number of polyunsaturated bonds per fatty-acyl chain (nPU/FA), number of unsaturated fatty-acyl chains (nUFA), number of polyunsaturated bonds per unsaturated fatty-acyl chain (nPU/UFA), and mean chain length (MCL).

^{13}C-MRS

^{13}C-MRS data quantification was performed based on glycogen phantom data, as in previous work.[47] To correct for the variable distance between coil and liver, a correction factor was calculated using the signal from the glycogen phantom measured with increasing distance from the coil (from 0 to 3 cm) and the coil–liver distance as measured on the localizer images obtained in breath-hold.

The concentration of natural abundance glycogen was calculated as follows:

$$c_{\text{in vivo}}(t) = \frac{A_{\text{in vivo}}(t)}{A_{\text{in vivo,ref}}} \frac{A_{\text{phantom,ref}}}{A_{\text{phantom}}} f_d f_{T_1} f_{\text{NOE}} c_{\text{phantom}}$$

where $c_{\text{invivo}}(t)$ and c_{phantom} are the concentrations [mM] of glycogen in vivo at time t and in the phantom, respectively. $A_{\text{in vivo}}$ and A_{phantom} represent the total areas of the fitted ^{13}C glycogen C-1 resonance doublets in vivo and in the phantom, respectively. $A_{\text{in vivo, ref}}$ and $A_{\text{phantom, ref}}$ represent the respective estimated areas of the acetone reference peak, correcting for different coil loads. f_d stands for the correction factor for the coil–liver distance, f_{T_1} and f_{NOE} are correction factors for differences between phantom and in vivo setup in T_1 and NOE. Following previous work,[47] f_{T_1} was assumed to be 1. f_{NOE} was determined to be 1.26 for our setup.

DMI

The natural abundance HDO signal was used as internal reference using an HDO concentration in liver of 8.94 mM.[32] For dynamic evaluations, the initial water signal was used as reference for all time points. A correction factor for T_1 relaxation was calculated from the estimated T_1 values of HDO and D-Glc. Given the short acquisition delay, no T_2 correction was applied.

The methods used for data acquisition and processing of the whole study are summarized in the standardized form of Lin et al.[48] in Table S1.

RESULTS

^{1}H-MRS

Typical results for the comparison of the ^{1}H-MR acquisition parameters with regard to the use of different echo times, WS techniques, and RS methods are depicted in Figure 1. The CMRR-STEAM sequence proved to provide spectra of excellent quality for very short echo times of 6–7 ms, and comparison with spectra obtained with 14 ms T_E did in general show a small benefit in intensities but also that broad signals may provide a stronger base component that is more difficult to model. The most substantial difference in intensity is observed for the TMA peak at 3.2 ppm, which appears to be even larger in this subject than expected based on T_2 times from the literature[21] ($T_2 = 32$ ms, expected 23% signal loss from 6 versus 14 ms T_E). Comparison of VAPOR WS with water elimination by MC indicates that water signal removal was usually more effective with VAPOR, but that the water reference acquired with MC can be useful for compensation of motion-induced phase and frequency variation, though this feature is mostly relevant for very small VOIs[49–60] and here for subjects with low fat content. Comparison of spectra acquired in breath-holds versus those obtained with rhythmic breathing indicates that both acquisition schemes are viable, but that the latter provided more stable and robust results in most subjects. A quantitative evaluation of resulting parameters for lipid characterization as obtained from several subjects as functions of acquisition mode is given in Table S1,S2.

Figure 2 illustrates the model fit of hepatic spectra for a single case, documenting the evaluation of lipid composition. In Figure 2B, it is seen that the metabolite signals in the range of 3.3–4 ppm can be well fitted with small-metabolite base spectra and an experimental glycogen base spectrum. However, given the low resolution, the potential residual water signal, and the severe overlap of spectra from glycogen, Glc, and the nonmethyl parts of choline, GPC, PCho, and betaine, a clear identification and quantification of any of these metabolite contributions is impossible. The lipid composition parameters for chain length and saturation can be well derived from these spectra and are given for the illustrated subject in Figure 2C. Numerical results from all the subjects considered are in line with expectations from the literature.[51] An exponential relationship between HLC and BMI and a linear relationship* between MCL and BMI of the subjects was found and is shown in Figure S3.

^{13}C-MRS

^{13}C-MRS acquisition parameters were evaluated, including T_R, NOE parameters, and total scan time per time point. The properties of the adiabatic excitation pulse were verified in vitro in a small oil phantom at the center of the heteronuclear coils in terms of signal independence of RF power beyond a threshold voltage (~180 V, Figure 3A) and signal independence of pulse length within an adiabatic regime (Figure 3B). Using a more extended glycogen phantom, optimal settings for T_R and NOE voltage were probed within a SAR-allowed parameter space. NOE increased the available signal by ~15% (Figure 3C,D), a signal gain that could not be achieved by reducing T_R with lower voltage for NOE irradiation or no NOE at all. With the short T_1 of glycogen, the shortest attainable T_R yields the highest SNR efficiency (Figure 3C). Figure 3E,F confirms the in vitro findings and extends to the in vivo situation. A minimum pulse length of 2 ms for the AHP is needed to assure maximum signal yield. The benefit of

(A)

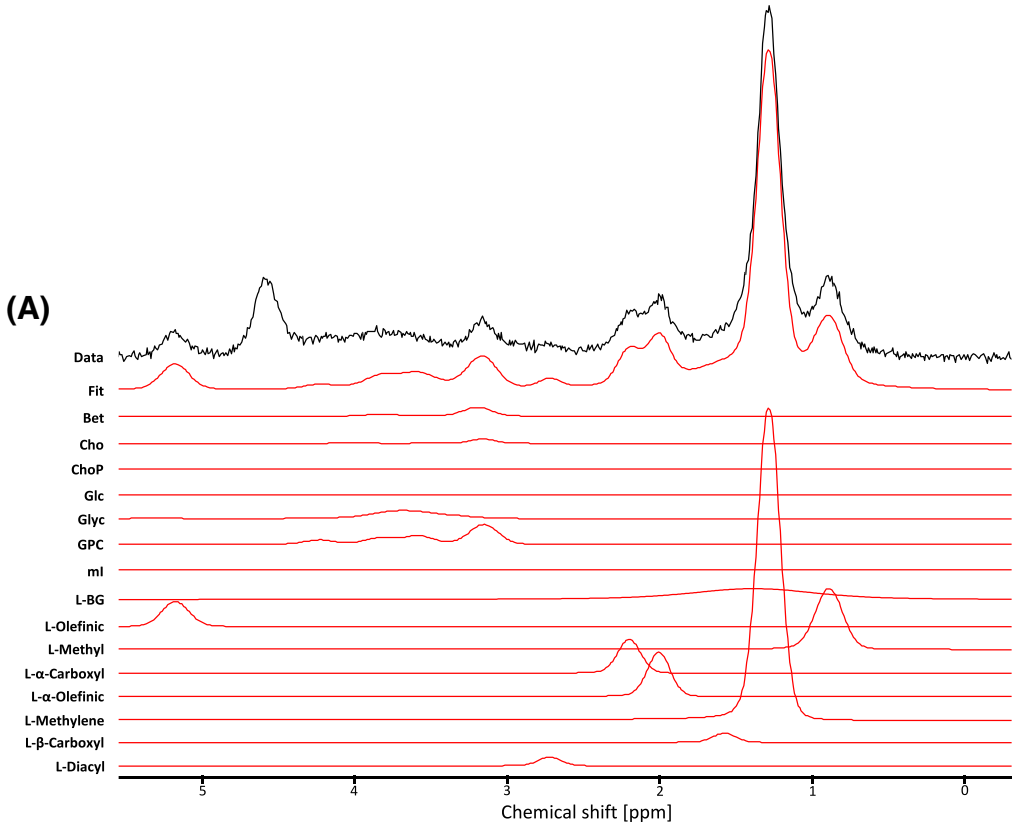

(B)

	HCL	SI	ndb	nPU/FA	nUFA	nPU/UFA	MCL
CMRR-STEAM, TE 06, VAPOR	1.27 ± 0.01%	7.4 ± 0.1	0.62 ± 0.03	0.30 ± 0.02	51.4 ± 0.1%	0.30 ± 0.02	13.8 ± 0.2
CMRR-STEAM, TE 14, VAPOR	1.74 ± 0.03%	6.5 ± 0.1	0.49 ± 0.04	0.20 ± 0.03	42.1 ± 1.9%	0.20 ± 0.03	12.4 ± 0.2
MC-STEAM, TE 14, breath-hold	1.29 ± 0.08%	6.6 ± 0.2	0.69 ± 0.02	0.34 ± 0.02	50.2 ± 6.9%	0.35 ± 0.02	13.20 ± 0.02
MC-STEAM, TE 14, breath-syncr.	1.27 ± 0.05%	7.3 ± 0.1	0.7 ± 0.1	0.39 ± 0.01	61.0 ± 10.8%	0.40 ± 0.01	14.2 ± 0.7

FIGURE 2 Illustration of model fitting and quantitative analysis of hepatic ^{1}H-MR spectra in a single subject. A, Experimental spectrum and linear-combination model fit with base spectra as listed in Section 2 and represented with estimated intensities for this case. B, Table with numerical estimates from two spectra each (within session repeat) from one subject for HLC, SI, ndb, nPU/FA, nUFA, nPU/UFA, and MCL.

NOE with 12 V irradiation is confirmed, though the NOE effect seems larger in vivo (44%) than in vitro (14%). Again, the best SNR per unit time is obtained for the shortest allowed T_R, while addition of an OVS pulse to eliminate potential glycogen signal from superficial muscle showed little effect. Comparing T_R values of 450 and 600 ms indicates an approximately 10% sensitivity gain for the shorter T_R—though with the uncertainty that for different loading conditions the shorter T_R might not be attainable.

Use of the thus defined acquisition parameters is illustrated by kinetic data in a cohort of five subjects, where detailed results for one subject are given in Figure 4 and data from the cohort further below. Figure 4A contains a ^{1}H-MR image, illustrating coil placement, location of the external standard, and a sketch of the receive profile. Figure 4B contains a typical ^{13}C-MR spectrum for a single time point with the glycogen doublet at 100.5 ppm and lipid resonances elsewhere (though removed by HLSVD before fitting). Glycogen SNR (peak height versus noise standard deviation in frequency domain) was approximately10 for each spectrum, and the doublet was always well resolved. Figure 4C shows 10 zoomed sample spectra selected from the whole time course from a single subject. Figure 4D contains the time evolution of the quantified glycogen content, indicating a small increase from baseline. Spectra were recorded for 150 min after D-Glc intake, starting with a glycogen content at baseline of 269 mM. For the last two acquisitions (140–150 min after D-Glc intake) the tissue content increased to 305 mM, corresponding to a 12% increase. From this series of spectra and the linear model of time evolution, a precision uncertainty of each measurement was calculated as the mean deviation from the linear trend. For this subject the estimated uncertainty was 21 mM glycosyl units, and for all five subjects studied the precision uncertainty turned out to be 20 ± 6 mM.

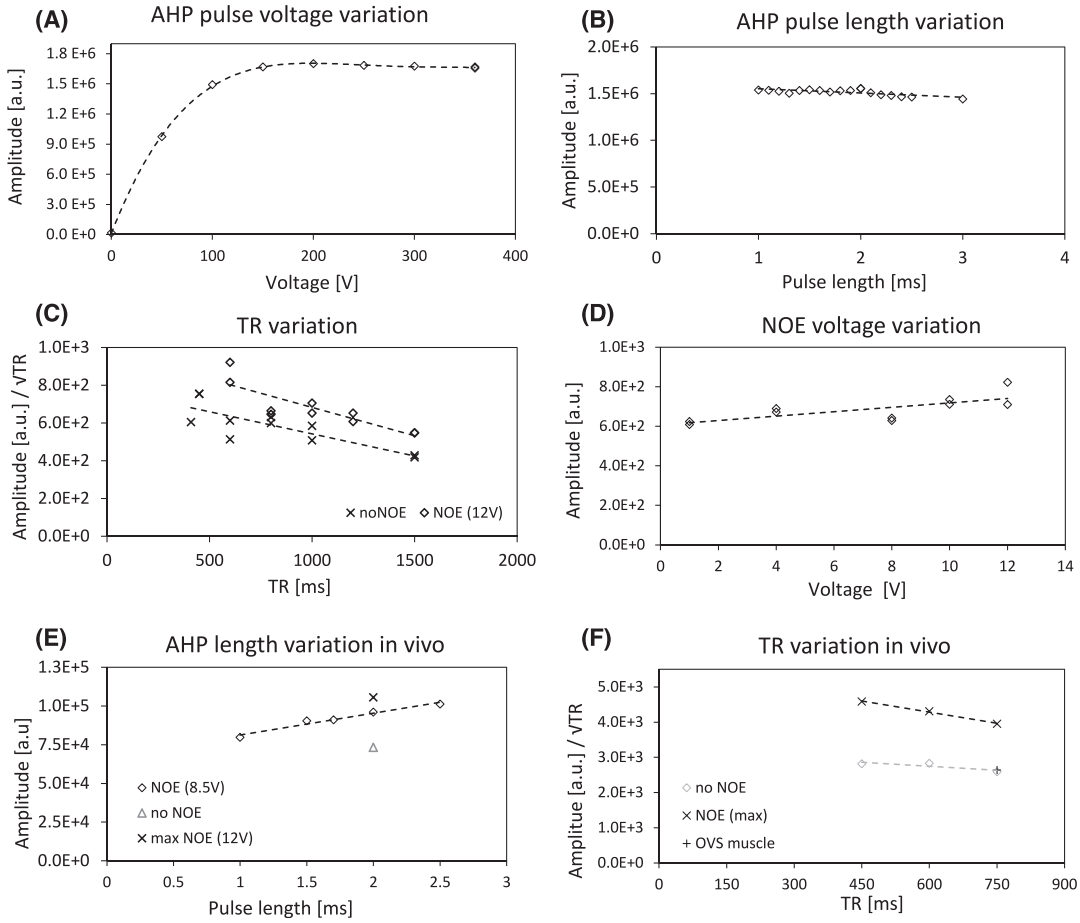

FIGURE 3 Evaluation results for acquisition parameters for ^{13}C-MRS. A,B, Verification of the expected properties for the AHP in vitro on an oil phantom with determination of minimum RF power needed (at 2 ms pulse length) (A) and investigation of influence of AHP length (at maximum voltage) (B). C,D, Results from a glycogen phantom. C, Results obtained with different T_R values, both without and with NOE (at maximum voltage where the minimum achievable T_R was limited to 600 ms due to SAR restrictions); D, in vitro dependence on NOE power. E,F, In vivo results. E, Variation of AHP length, with comparisons between cases without NOE, with NOE at 8.5 V, and with NOE at maximum voltage. F, Variation of T_R, including comparisons with and without NOE, and with and without OVS on the superficial thoracic muscle region.

DMI

DMI acquisition parameters were assessed, including excitation pulse type, duration, and voltage, T_R, length of phase-encoding gradient, and number of acquisitions needed per time point. Figure 5A,B shows in vitro evaluations, where excitation pulse type, duration (constant flip angle in the hard-pulse case), and voltage were varied. Figure 5C compares signal intensity for voxels progressively more distant from the coil for different excitation pulses, where a hard pulse with a 0.5 ms length and 291 V voltage performs best. In vivo, similar results were obtained. Variation of the hard-pulse voltage (Figure 5D) shows optimal performance at the relevant depth in this subject at about 200 V, though this depends on coil loading. Figure 5E mirrors Figure 5C in vivo, showing that the rectangular pulse gives slightly more signal than the adiabatic pulse. For three subjects, T_R was varied after D-Glc intake for T_1 evaluation. T_1 was estimated to be 85 ± 8 ms for D-Glc and 341 ± 14 ms for HDO. Corresponding data for one subject are reported in Figure 5F,G.

Using a parameter setup expected to yield robust results in a clinical study, kinetic hepatic DMI data were obtained and are illustrated for a single subject in Figure 6. Figure 6A shows the nominal MRSI grid overlaid on an axial localizer image and Figure 6B the spectral quality in a spectrum from a single pixel (nominal resolution of 18.3 × 18.3 × 27.5 mm^3) near the coil's center (SNR ∼34, linewidth ∼21 Hz), documenting the very good signal separation between the HDO (4.7 ppm) and D-Glc (3.7 ppm) signals. In nonobese subjects, about 154 voxels (∼800 cm^3) within the liver show an HDO peak with SNR > 5 and a full-width at half-maximum (FWHM) of about 25 Hz. Figure 6C,D demonstrates the temporal evolution of the spectra and the quantified signals, as recorded with a resolution between 4 and 9 min, in relation to the measured peripheral total and deuterated blood Glc content.

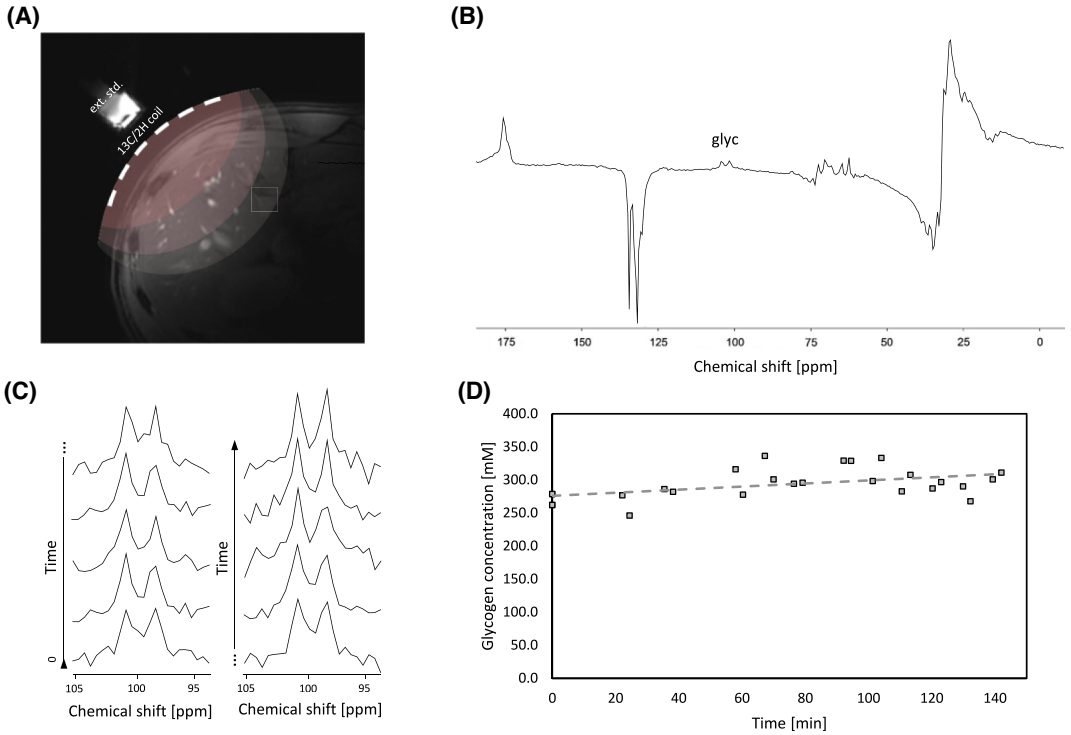

FIGURE 4 Illustration of dynamic ^{13}C-MRS after an oral Glc load in a single healthy subject. A, Anatomical image illustrating the positioning of the coil and its sensitivity, with an external standard located at the back of the coil. B, ^{13}C-MR spectrum obtained by pulse and acquire from the entire sensitive area of the coil, revealing the presence of the glycogen (glyc) doublet at 100.5 ppm. C, Ten zoomed-in sample spectra of glycogen, selected from the entire time course for this participant (spectra plotted without apodization). D, Fitted signal of the glycogen doublet, indicating a linear increase of about 12% compared with baseline (from 214 to 242 mM).

Similarly to the approach used for ^{13}C-MRS, the precision of single time point measurements was determined as the mean deviation of the quantified tissue content from a model time course. Here, a linear model of water content between time 0 and 40 min was used. For the volunteer in Figure 6, the precision of water quantification (which most likely applies also to D-Glc) came out as 0.07 mM, while for the whole cohort it was 0.22 ± 0.18 mM.

Figure 7 summarizes the kinetic data from DMI and ^{13}C-MRS for an initial cohort of five healthy subjects. The temporal courses are quite different between subjects but indicate that the hepatic glycogen content increases at maximum by about 10%–15% within 150 min after intake, which for an average liver volume would correspond to about 6–8 g of ingested Glc, that is, about 10%–15% of the administered dose. From DMI, one can approximate an average concentration of about 1–2 mM D-Glc, which with the same approximations would correspond to an amount of about 0.2–0.5 g D-Glc for the whole liver.

Figure 8 demonstrates spatial heterogeneity in the buildup of the D-Glc tissue content. Metabolic maps were constructed for different time points after Glc intake at time T0. They represent the ratio of the time-dependent D-Glc versus the initial HDO signal and thus depict the spatially inhomogeneous uptake of D-Glc. Substantial Glc hyperintensities are evident early on in the medial part of the liver and are likely due to partial coverage of the portal vein delivering the ingested Glc from the gastrointestinal tract. This is corroborated in Figure 7B, which shows time courses for different positions. Hepatic regions with only a few large blood vessels feature a rise of the signal until about T70, with the signal remaining visible until the end of the scan. Voxel 4 is selected to overlap with large vessels in the liver hilus region, as documented by the background image obtained in end-expiration, while the D-Glc map is smeared due to free breathing. It shows a more rapid increase, reaching its maximum at T50 before the signal drops to baseline and is not visible toward the end.

DISCUSSION

In this work, we present the use of a trinuclear dynamic MR examination for the noninvasive and nonradioactive investigation of hepatic carbohydrate and lipid metabolisms in humans. ^{1}H-MR is applied to correlate metabolic activity with anatomical regions through the acquisition of images and to determine intrahepatic lipid profiles. ^{2}H-MRSI provides spatially resolved measurements of ingested, ^{2}H-labelled glucose and ^{13}C-MRS serves to document hepatic glycogen levels and changes thereof. A triple-tuned RF coil is the basis for uninterrupted interleaved examination of

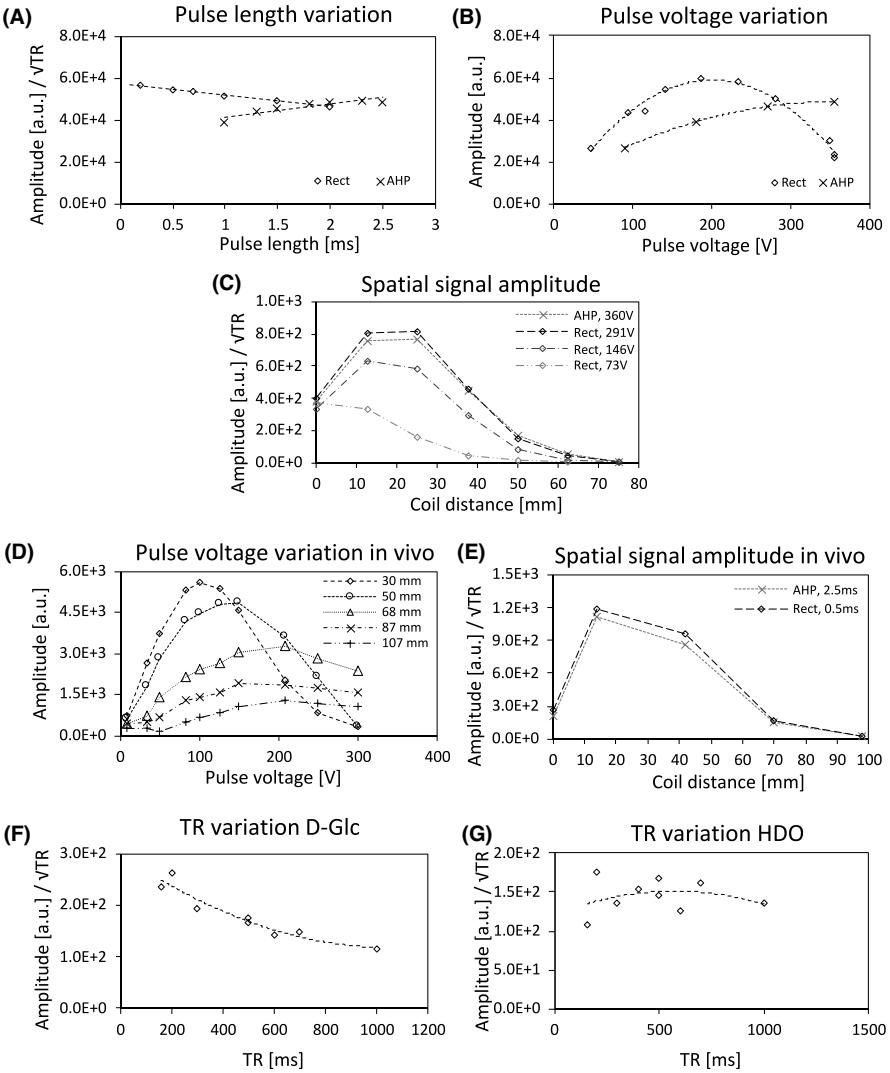

FIGURE 5 Evaluation results for acquisition parameters for DMI. A–C, In vitro results; D–G, in vivo measurements. A, Results from varying pulse lengths, where for the hard pulse the flip angle was kept constant, but for the AHP the maximum voltage was kept constant. B, Outcome for pulse voltage variation at constant pulse duration for the rectangular pulse (0.5 ms) and the AHP (2 ms) with the expected result of change of flip angle for the hard-pulse case and reaching maximum signal with higher voltage for the AHP. C, Spatial dependence of signal amplitude upon variation of pulse power for the hard pulse and AHP. D, In vivo pulse power dependence of signal amplitude at various distances from the RF coil. E, Comparison of the receive profile for a hard pulse and an AHP in vivo. F,G, T_R dependence of signal for D-Glc and HDO in a single subject.

these metabolic processes and the MR methods were chosen for robust results in clinical research applications. Preliminary physiological results in healthy volunteers are described for all three nuclei to provide proof of concept and feasibility, but more extended studies are needed for solid claims in terms of (patho-)physiology.

The basic requirement for the acquisition of data from three nuclei without moving the patient is the use of a triple-tuned RF coil, which results in some compromises with regard to SNR and B_1^+ efficiency. Because of lack of availability of comparable results with double-tuned coils at 7T, the loss in SNR can only be estimated. Given that the ratio between the resonance frequencies for the current case is not very different than for a triple-tuned coil tuned to $^{1}H/^{31}P/^{13}C$ that had been built with a similar geometry for 3 T previously and has been described in previous work,[51] one can expect a similar loss in B_1^+ efficiency for ^{13}C and ^{2}H in the current case, that is, a 1.5 times lower B_1^+ field in the triple-tuned case than in double-tuned $^{31}P/^{1}H$ and $^{13}C/^{1}H$ coils with similar geometries. For B_1^+ this is not crucial as long as enough RF power is available to achieve the needed flip angles, though higher power requirements exacerbate SAR limits. It can be expected that the B_1^- efficiency suffers a similar loss, indicating that for equal SNR approximately two times longer data acquisition is needed for both heteronuclei.

The methods for all three nuclei were selected and optimized with specific criteria in mind, but variants thereof might be preferred with other targets in focus.

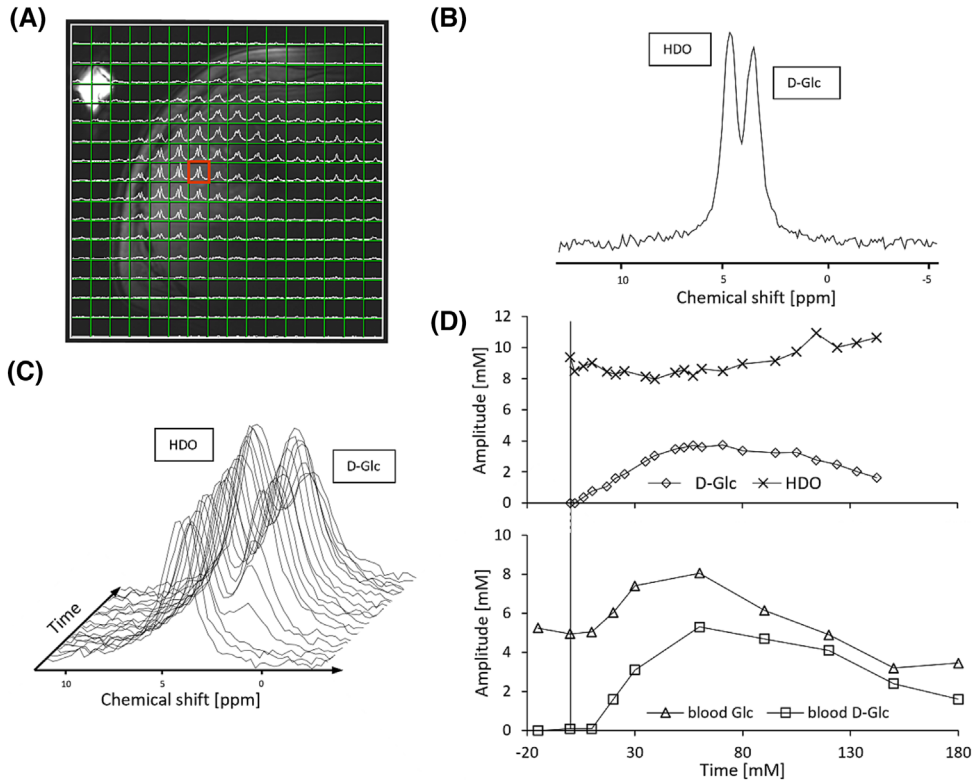

FIGURE 6 Illustration of dynamic DMI after an oral Glc load in a single healthy subject. A, Anatomical image overlaid with the nominal MRSI grid, consisting of 16 × 16 voxels per slice after zero-filling. B, ^{2}H-MRSI signal obtained from a single central 13.7 × 13.7 × 18.3 mm^{3} voxel. C, Time evolution of spectra, where each spectrum represents the average of six central voxels. D, Estimated tissue content of hepatic D-Glc and HDO as well as deuterated and total blood glucose concentration. The hepatic D-Glc peak builds up within minutes after [6,6'-$^{2}H_{2}$]-Glc intake, followed immediately by the surge of the D-Glc signal in peripheral venous blood. Hepatic D-Glc reaches a maximum at 60–70 min and subsequently decreases.

For ^{1}H-MRS, the evaluation concerned the localization method, the T_E, the WS technique, and the type of motion synchronization. Given the limited B_1^+ strength of the surface coil and its inhomogeneity, it was obvious from the start that STEAM would be superior to spin-echo based methods. The results for optimal choice of T_E are inconclusive. The STEAM sequence available from CMRR was shown to provide clean spectra with T_E as short as 6 ms, most useful for investigation of the water and TMA signal because of their very short T_2 values (T_2 = 15 ms for water and T_2 = 32 ms for TMA)[21] and also for an exploration of the potential of ^{1}H-MRS to determine glycogen levels, while for evaluation of the lipid profile a longer T_E may be beneficial because of the sufficiently long T_2 values of these compounds and the inherent water signal reduction at longer T_E. A reduced water signal is particularly beneficial for clear quantification of the olefinic lipid peak at the foot of the water signal. The use of MC instead of VAPOR WS is generally recommended for cases with substantial shot-to-shot signal fluctuations[53] or if very-small-metabolite signals are observed that do not provide enough signal for robust phase and frequency alignment of single acquisitions.[50,53,54] None of this is the case here, such that the superior WS efficiency of VAPOR may seem attractive (unless glycogen signals with potential signal loss due to NOE magnetization transfer are targeted[15]). Previous studies of hepatic MRS at 7T have suggested non-water-suppressed MRS (with a special gradient compensation method to enable non-water-suppressed MRS).[20] Though this method has not been directly compared in this study, it appears that WS or MC may be superior for the clean definition of the olefinic peak, in particular in cases of nonideal shim (e.g., asymmetric line shape) or elevated hepatic iron content. If, however, frequency-selective pulses are used for WS or metabolite inversion, it is of importance to effectively freeze the breathing motion with its implicated shift in resonance frequency. An earlier study[17] has shown some benefit for MC versus VAPOR in terms of reproducibility in spite of the less efficient WS efficacy. While that study,[17] using a body transmit coil, did not try to quantify the olefinic proton signal, which would be a clear disadvantage for MC, the current setup did allow for quantification of this peak. In the current study, two respiration-synchronization methods have been compared: (1) 14–15 s of breath-hold and (2) voluntary synchronization with the scanner to inspire and expire after each acquisition and to remain in expiration for the subsequent acquisition. Triggering from a signal of a respiration belt or navigator-triggered acquisitions were not tested. The use of a navigator signal to follow the motion of the diaphragm is difficult with a surface coil with limited field of view, and respirator-belt triggering would have been feasible but is known to often lead to inconsistent expiration positions. Both tested methods worked well in this cohort of healthy subjects, with rhythmic breathing often yielding somewhat better resolved spectra.

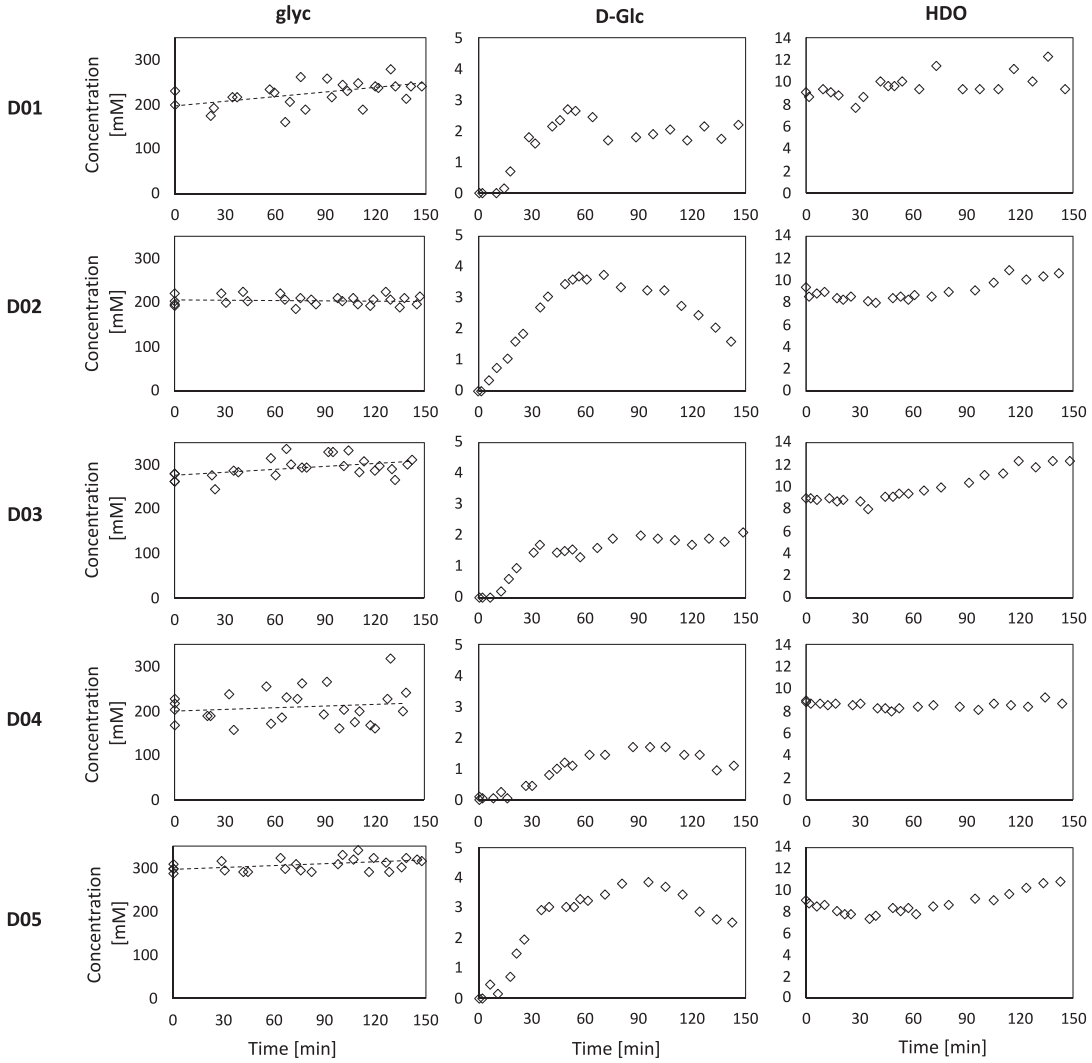

FIGURE 7 Results for DMI and ^{13}C-MRS from a pilot study following five healthy subjects after D-Glc intake. Time courses for glycogen (glyc), D-Glc, and HDO (subjects labelled as D01–D05). Linear trend lines were estimated for glyc.

The breath-hold method limits the number of acquisitions and necessitates short T_R (with potential for a drift of signal toward the end of the breath-hold and for inconsistent breath-hold positions if the signal from multiple breath-holds were to be combined). SNR from a few acquisitions is often sufficient for the study of lipid signals but is insufficient for robust quantification of small molecular metabolites. In addition, a 16-step phase cycle is too long for a breath-hold; hence one has to either revert to shorter phase cycles or split the phase-cycle into multiple breath-holds, which is not ideal if the breathing position is not identical.

Rhythmic breathing on the other hand is not possible with patients who may be short of breath or too tense for relaxed breathing. It was not possible to quantify glycogen from ^{1}H-MRS in these measurements, and it is even difficult to say whether this is possible in principle at this field strength. The spectral area between 3.4 and 4.1 ppm was ill resolved, the signals from glycogen and Glc overlap strongly (one might enforce a concentration limit for the Glc contribution), and in addition myo-inositol and the non-TMA signals of all the TMA-group-bearing metabolites also have signals in that spectral region, where the TMA peak can thus be fitted only with great uncertainty regarding its composition between Cho, PCho, GPC, and betaine. Dedicated scans with parallel determination of glycogen levels by ^{13}C-MRS and as a function of glycogen loading are needed to judge the potential of ^{1}H-MRS for quantitative glycogen determination. The final listed fitting results were therefore limited to lipid characterization.

The methodology for ^{13}C-MRS to determine glycogen levels followed closely the method suggested by Buehler et al.[47] for 3T scans. However, a considerably larger SAR load from the adiabatic pulse at 7T than at 3 T prevented the use of ^{1}H decoupling in combination with adiabatic excitation. This would necessitate much higher T_R values. In addition, the specific 7T scanner does not have the needed filters in place, such that decoupling introduces additional noise in the ^{13}C channel. Furthermore, the more inhomogeneous B_1^+ profile at 7T would lead to very inhomogeneous decoupling efficiency for CW decoupling, leading to unpredictable glycogen lineshapes. However, the lack of decoupling did not really

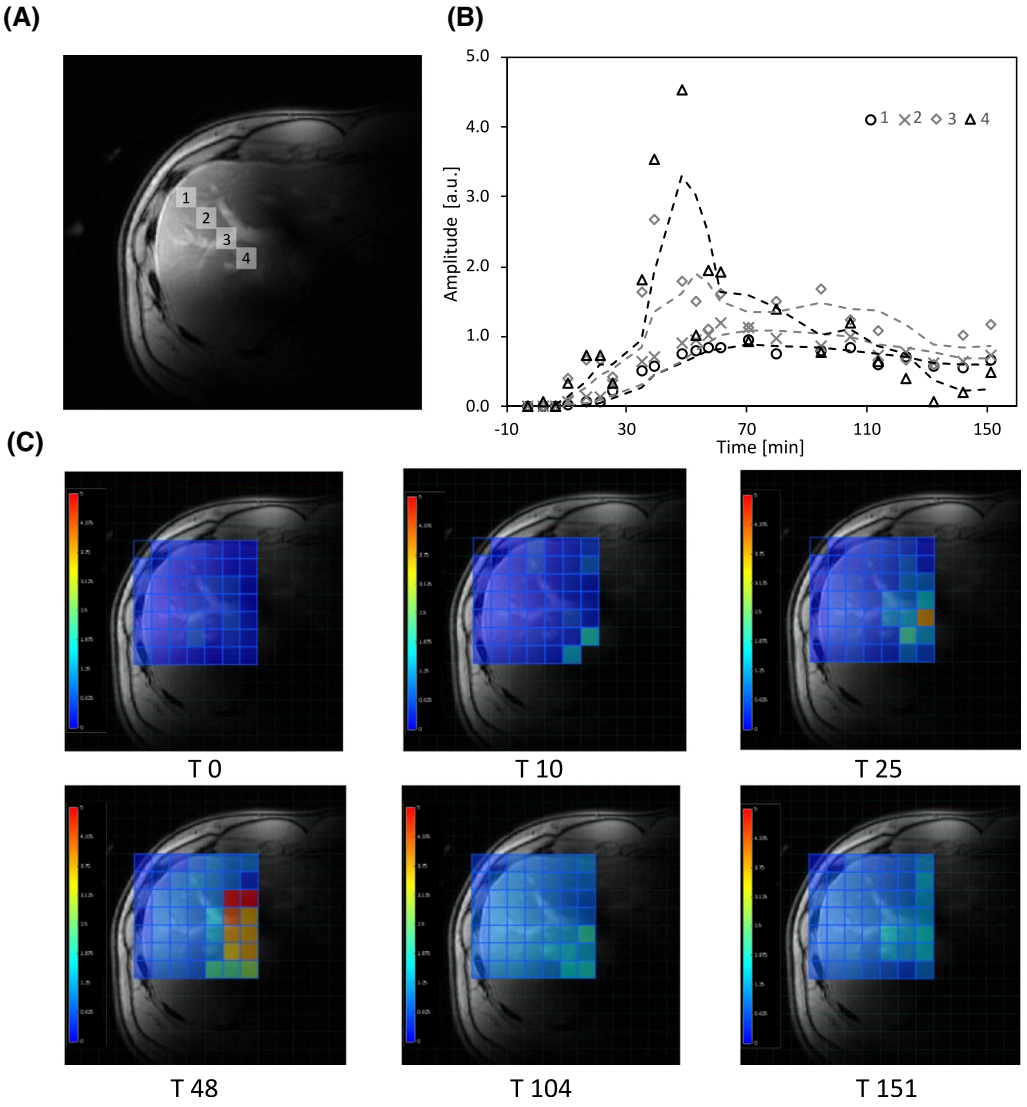

FIGURE 8 Illustration of spatial dependence of glucose buildup in the liver for a single slim healthy subject. A, Anatomical image overlaid with selected voxel positioning. B, Ratio between signals of D-Glc and HDO at baseline for the four indicated voxels at increasing distance from the coil. Voxels 1 and 2 are placed on mostly hepatic tissue (including capillaries). Voxel 4 is selected to overlap with hepatic hilum including large vessels, such as the portal vein. Voxel 3 is in an intermediate position. Dashed lines represent a two-period moving average. C, Kinetic metabolic maps of D-Glc over initial HDO signal. The grid is composed of a 7 × 7 grid (selected to focus on the hepatic region), overlapped with anatomical images. The metabolic maps are shown before and 10, 25, 48, 104, and 151 min after [6,6'-$^{2}H_2$]-Glc intake, demonstrating spatially heterogeneous signal with the earliest signal increase in the hilum region.

prove to be a problem since there is no signal overlap with other moieties (except for a tiny β-Glc signal; the lipid signals are well separated) and there is no prohibitive signal loss due to coupling evolution for short dead times after adiabatic excitation. Hence, fitting using a model with the peak splitting as prior knowledge essentially yields estimation errors that are not too different from those for a singlet. Basic simulations showed that the Cramér–Rao lower bounds are about 25% higher without decoupling. The use of a hard pulse would have allowed us to use a shorter T_R with significant SNR gain, but this would have been more difficult for absolute quantification, where coil loading would have had a bigger impact. Effectively, the parameter optimization was governed by SAR limits, where the length of the adiabatic pulse and the magnitude of NOE voltage both increase the deposited RF power, while only extending the T_R can be used to lower the SAR load.

The feasibility checks were done mostly in nonobese subjects and sensitivity would definitely drop for subjects with a lot of subcutaneous fat over the liver, though we did not find a prohibitive signal drop for our most obese subject with a BMI of 30.0 kg/m^2 in this study and further measurements in another cohort (maximum BMI 34.2 kg/m^2).

The SNR and thus minimal scan time per spectrum (resolution of the time course) could of course be improved with the use of additional ^{13}C labelling of the ingested Glc. However, this would not only make the investigation much more expensive but would also influence and potentially

complicate the interpretation of the glycogen data in that mainly glycogen buildup from the newly ingested Glc would be measurable, and synthesis and turnover of baseline glycogen and Glc would essentially go unnoticed.

For DMI, a plain conventional MRSI sequence with hard-pulse excitation has been chosen. It provides excellent SNR per time point for a region-of-interest analysis without detailed intrahepatic region analysis. Adiabatic excitation did not improve SNR for most areas and, given the valid intrahepatic concentration standard of natural abundance HDO, excitation and receive inhomogeneities expected based on the B_1^+ profiles did not play a major role. The weighted-acquisition scheme helped substantially to limit scan time at reasonable resolution even without reducing T_R too much into a regime where knowledge of T_1 of HDO (T_1 is much longer for HDO than D-Glc) would be crucial for proper quantification. Despite the use of a surface coil, a reasonable coverage of a large part of the liver could be obtained—at least in nonobese subjects (but of course by no means reaching the field of view offered by a body coil arrangement[55]). It even allowed depth resolved Glc dynamics to be obtained. However, without doubt, use of an echo-planar readout for one spatial direction would be beneficial[56] to increase either the temporal or spatial resolution, which would be particularly important to define a portal vein input function for metabolic modeling. At the current resolution it is not possible to clearly distinguish between hepatocellular and vascular glucose contributions on a macroscopic, let alone mesoscopic, scale. The flip angle was not optimized for each subject for time reasons, but this could improve SNR considerably in cases with unusual coil loadings. No downstream metabolites (glutamate or lactate) have been observed, either directly in single spectra, or in overall summed spectra of the whole observed liver, or if multiple spectra from the whole time course were added up or some of them combined from multiple subjects.

The methodology was tested in a small cohort of healthy subjects, providing first physiological insights that are worthwhile to mention, but must all be verified in a larger cohort.

- *^{1}H-MRS*. The lipid characteristics conform mostly to previous findings reported in the literature. Correlating all the results (all volunteer data, independent of methods used) with relevant subject characteristics, the unsurprising exponential increase of total lipid content with BMI was confirmed. However, also the less strongly founded linear relation between BMI and MCL could be verified, while a negative correlation between unsaturation index and lipid content[17] was not clearly evident from our data. (Results demonstrated in Figure S3.) Obviously, a study in a larger cohort and with uniform methodology is needed to prove and extend previous findings.
- *Dynamic DMI*. D-Glc load experiments showed a surprisingly large spread of results for the kinetic behavior of D-Glc and HDO time course signals. This will have to be related to blood Glc dynamics and further clinical data derived from plasma glucose enrichment data (illustrated for one case in Figure 6). Simultaneous observation of D-Glc levels in stomach and intestines as possible with a whole-body coil[55] would allow for inclusion of glucose absorption kinetics in metabolic models. The use of different Glc loads would provide further relevant physiological as well as practical insights and lead to substantial lowering of tracer costs.[57]
- *Dynamic ^{13}C-MRS*. Similarly to the DMI results, also the prandial change in glycogen levels varied substantially between subjects, though it seems that a maximum increase of about 10%–15% in glycogen level within 150 min after ingestion is to be observed with the current setup, where no rigorous depletion of glycogen had been enforced.

In conclusion, a trinuclear interleaved dynamic MR examination combining ^{1}H-MRS, ^{13}C-MRS, and DMI is a promising approach to investigate lipid and carbohydrate metabolism in a single-session ultra-high-field experimental setup. First findings in healthy volunteers suggest that the dynamics of ingested glucose in the liver can be excellently mapped using ^{2}H-MRSI alongside evaluations of lipid content detected by ^{1}H-MRS, while the determination of changes in glycogen levels by ^{13}C-MRS is more limited by SNR even at 7T. Though the methodology is ready for clinical research investigations, improvements can still be envisaged, with resolution gain for DMI using echo-planar readouts, potential SNR improvements from temporal denoising methods for ^{13}C-MRS,[58,59] and real-time interleaving of multinuclear methods[60] as first targets. Mechanistic conclusions from the suggested imaging methodology can be augmented with complementary assessments, such as blood sampling for hormones and metabolites, use of additional tracers, clamp protocols, and most importantly development of metabolic models to quantify key metabolic parameters.

ACKNOWLEDGMENTS

Supported by the Swiss National Science Foundation (PCEGP3_186978) and the Diabetes Center Bern. We further acknowledge the support received from the study nurse team (Valérie Brägger, Joana Filipa Rodrigues Cunha Freitas, Sandra Tenisch), Andreas Melmer, and Laura Goetschi from the Department of Diabetes, Endocrinology, Nutritional Medicine and Metabolism, Inselspital, Bern University Hospital. Open access funding provided by Universitat Bern.

ORCID

Simone Poli https://orcid.org/0000-0001-5676-3187
Naomi F. Lange https://orcid.org/0000-0002-9519-4949
Michele Schiavon https://orcid.org/0000-0003-0590-2399
David Herzig https://orcid.org/0000-0003-1028-9445

Chiara Dalla Man https://orcid.org/0000-0002-4908-0596
Lia Bally https://orcid.org/0000-0003-1993-7672
Roland Kreis https://orcid.org/0000-0002-8618-6875

ENDNOTES

* Statistically significant when all data are pooled, irrespective of acquisition modes.

REFERENCES

1. Smith GI, Shankaran M, Yoshino M, et al. Insulin resistance drives hepatic de novo lipogenesis in nonalcoholic fatty liver disease. *J Clin Invest*. 2020; 130(3):1453-1460. doi:10.1172/JCI134165
2. Krssak M, Roden M. The role of lipid accumulation in liver and muscle for insulin resistance and type 2 diabetes mellitus in humans. *Rev Endocr Metab Disord*. 2004;5(2):127-134. doi:10.1023/B:REMD.0000021434.98627.dc
3. Petersen MC, Vatner DF, Shulman GI. Regulation of hepatic glucose metabolism in health and disease. *Nat Rev Endocrinol*. 2017;13(10):572-587. doi: 10.1038/nrendo.2017.80
4. Perry RJ, Samuel VT, Petersen KF, Shulman GI. The role of hepatic lipids in hepatic insulin resistance and type 2 diabetes. *Nature*. 2014;510(7503):84-91. doi:10.1038/nature13478
5. Jones JG. Non-invasive analysis of human liver metabolism by magnetic resonance spectroscopy. *Metabolites*. 2021;11(11):751. doi:10.3390/metabo11110751
6. Gursan A, Prompers JJ. Magnetic resonance imaging and spectroscopy methods to study hepatic glucose metabolism and their applications in the healthy and diabetic liver. *Metabolites*. 2022;12(12):1223. doi:10.3390/metabo12121223
7. Burian M, Hajek M, Sedivy P, Mikova I, Trunecka P, Dezortova M. Lipid profile and hepatic fat content measured by 1H MR spectroscopy in patients before and after liver transplantation. *Metabolites*. 2021;11(9):625. doi:10.3390/metabo11090625
8. Neeland IJ, Ross R, Després JP, et al. Visceral and ectopic fat, atherosclerosis, and cardiometabolic disease: a position statement. *Lancet Diabetes Endocrinol*. 2019;7(9):715-725. doi:10.1016/S2213-8587(19)30084-1
9. Hwang JH, Choi CS. Use of in vivo magnetic resonance spectroscopy for studying metabolic diseases. *Exp Mol Med*. 2015;47(2):e139-e139. doi:10.1038/emm.2014.101
10. Longo R, Pollesello P, Ricci C, et al. Proton MR spectroscopy in quantitative in vivo determination of fat content in human liver steatosis. *J Magn Reson Imaging*. 1995;5(3):281-285. doi:10.1002/jmri.1880050311
11. Szczepaniak LS, Babcock EE, Schick F, et al. Measurement of intracellular triglyceride stores by H spectroscopy: validation in vivo. *Am J Physiol*. 1999; 276(5):E977-E989. doi:10.1152/ajpendo.1999.276.5.E977
12. Ouwerkerk R, Pettigrew RI, Gharib AM. Liver metabolite concentrations measured with 1H MR spectroscopy. *Radiology*. 2012;265(2):565-575. doi: 10.1148/radiol.12112344
13. Weis J, Kullberg J, Ahlström H. Multiple breath-hold proton spectroscopy of human liver at 3T: relaxation times and concentrations of glycogen, choline, and lipids. *J Magn Reson Imaging*. 2018;47(2):410-417. doi:10.1002/jmri.25734
14. van Zijl PCM, Jones CK, Ren J, Malloy CR, Sherry AD. MRI detection of glycogen in vivo by using chemical exchange saturation transfer imaging (glycoCEST). *Proc Natl Acad Sci U S A*. 2007;104(11):4359-4364. doi:10.1073/pnas.0700281104
15. Zhou Y, van Zijl PCM, Xu X, et al. Magnetic resonance imaging of glycogen using its magnetic coupling with water. *Proc Natl Acad Sci U S A*. 2020; 117(6):3144-3149. doi:10.1073/pnas.1909921117
16. Walker-Samuel S, Ramasawmy R, Torrealdea F, et al. In vivo imaging of glucose uptake and metabolism in tumors. *Nat Med*. 2013;19(8):1067-1072. doi:10.1038/nm.3252
17. Xavier A, Arteaga de Castro C, Andia ME, et al. Metabolite cycled liver 1H MRS on a 7T parallel transmit system. *NMR Biomed*. 2020;33(8):e4343. doi:10.1002/nbm.4343
18. Dreher W, Leibfritz D. New method for the simultaneous detection of metabolites and water in localized in vivo 1H nuclear magnetic resonance spectroscopy. *Magn Reson Med*. 2005;54(1):190-195. doi:10.1002/mrm.20549
19. MacMillan EL, Chong DGQ, Dreher W, Henning A, Boesch C, Kreis R. Magnetization exchange with water and T1 relaxation of the downfield resonances in human brain spectra at 3.0 T. *Magn Reson Med*. 2011;65(5):1239-1246. doi:10.1002/mrm.22813
20. Gajdošík M, Chadzynski GL, Hangel G, et al. Ultrashort-TE stimulated echo acquisition mode (STEAM) improves the quantification of lipids and fatty acid chain unsaturation in the human liver at 7 T. *NMR Biomed*. 2015;28(10):1283-1293. doi:10.1002/nbm.3382
21. Gajdošík M, Chmelík M, Just-Kukurová I, et al. In vivo relaxation behavior of liver compounds at 7 Tesla, measured by single-voxel proton MR spectroscopy. *J Magn Reson Imaging*. 2014;40(6):1365-1374. doi:10.1002/jmri.24489
22. Kacerovsky M, Jones J, Schmid AI, et al. Postprandial and fasting hepatic glucose fluxes in long-standing type 1 diabetes. *Diabetes*. 2011;60(6):1752-1758. doi:10.2337/db10-1001
23. Krssak M, Brehm A, Bernroider E, et al. Alterations in postprandial hepatic glycogen metabolism in type 2 diabetes. *Diabetes*. 2004;53(12):3048-3056. doi:10.2337/diabetes.53.12.3048
24. Valette J, Tiret B, Boumezbeur F. Experimental strategies for in vivo 13C NMR spectroscopy. *Anal Biochem*. 2017;529:216-228. doi:10.1016/j.ab.2016.08.003
25. Kršśák M. ^{13}C MRS in human tissue. In: Harris, RK and Wasylishen, RL eds. *eMagRes*. Wiley; 2016:1027-1038. 10.1002/9780470034590.emrstm1490
26. Matyka K, Dixon RM, Mohn A, et al. Daytime liver glycogen accumulation, measured by 13C magnetic resonance spectroscopy, in young children with Type 1 diabetes mellitus. *Diabet Med*. 2001;18(8):659-662. doi:10.1046/j.0742-3071.2001.00560.x
27. Roden M, Perseghin G, Petersen KF, et al. The roles of insulin and glucagon in the regulation of hepatic glycogen synthesis and turnover in humans. *J Clin Invest*. 1996;97(3):642-648. doi:10.1172/JCI118460

28. de Graaf RA, Rothman DL, Behar KL. State-of-the-art direct 13C and indirect 1H-[13C] NMR spectroscopy in vivo. *NMR Biomed*. 2011;24(8):958-972. doi:10.1002/nbm.1761
29. Miller CO, Cao J, Zhu H, et al. 13C MRS studies of the control of hepatic glycogen metabolism at high magnetic fields. *Front Phys Ther*. 2017;5:21. doi:10.3389/fphy.2017.00021
30. Chen Ming Low J, Wright AJ, Hesse F, Cao J, Brindle KM. Metabolic imaging with deuterium labeled substrates. *Prog Nucl Magn Reson Spectrosc*. 2023;134/135:39-51. doi:10.1016/j.pnmrs.2023.02.002
31. Lu M, Zhu XH, Zhang Y, Mateescu G, Chen W. Quantitative assessment of brain glucose metabolic rates using in vivo deuterium magnetic resonance spectroscopy. *J Cereb Blood Flow Metab*. 2017;37(11):3518-3530. doi:10.1177/0271678X17706444
32. De Feyter HM, Behar KL, Corbin ZA, et al. Deuterium metabolic imaging (DMI) for MRI-based 3D mapping of metabolism in vivo. *Sci Adv*. 2018;4(8):eaat7314. doi:10.1126/sciadv.aat7314
33. Ruhm L, Avdievich N, Ziegs T, et al. Deuterium metabolic imaging in the human brain at 9.4 Tesla with high spatial and temporal resolution. *NeuroImage*. 2021;244:118639. doi:10.1016/j.neuroimage.2021.118639
34. Kreis F, Wright AJ, Hesse F, Fala M, Hu D, Brindle KM. Measuring tumor glycolytic flux in vivo by using fast deuterium MRI. *Radiology*. 2020;294(2):289-296. doi:10.1148/radiol.2019191242
35. Riis-Vestergaard MJ, Laustsen C, Mariager CØ, Schulte RF, Pedersen SB, Richelsen B. Glucose metabolism in brown adipose tissue determined by deuterium metabolic imaging in rats. *Int J Obes*. 2020;44(6):1417-1427. doi:10.1038/s41366-020-0533-7
36. Mahar R, Donabedian PL, Merritt ME. HDO production from [2H7]glucose quantitatively identifies Warburg metabolism. *Sci Rep*. 2020;10(1):8885. doi:10.1038/s41598-020-65839-8
37. de Graaf RA, Hendriks AD, Klomp DWJ, et al. On the magnetic field dependence of deuterium metabolic imaging. *NMR Biomed*. 2020;33(3):e4235. doi:10.1002/nbm.4235
38. De Feyter HM, Thomas MA, Behar KL, de Graaf RA. NMR visibility of deuterium-labeled liver glycogen in vivo. *Magn Reson Med*. 2021;86(1):62-68. doi:10.1002/mrm.28717
39. Poli S, Emara AF, Ballabani E, et al. Interleaved 1H-MRI, 2H-MRSI and 13C-MRS for time-resolved in vivo elucidation of glucose metabolism in human liver at 7 T. In: *Proceedings of the 31st Joint Annual Meeting ISMRM-ESMRMB*. 2022;628.
40. CMRR Spectroscopy Package. https://www.cmrr.umn.edu/spectro/
41. Döring A, Adalid V, Boesch C, Kreis R. Diffusion-weighted magnetic resonance spectroscopy boosted by simultaneously acquired water reference signals. *Magn Reson Med*. 2018;80(6):2326-2338. doi:10.1002/mrm.27222
42. Naressi A, Couturier C, Devos JM, et al. Java-based graphical user interface for the MRUI quantitation package. *Magn Reson Mater Phys Biol Med*. 2001;12(2/3):141-152. doi:10.1007/BF02668096
43. Pijnappel WWF, van den Boogaart A, de Beer R, van Ormondt D. SVD-based quantification of magnetic resonance signals. *J Magn Reson*. 1992;97(1):122-134. doi:10.1016/0022-2364(92)90241-X
44. Vanhamme L, van den Boogaart A, Van Huffel S. Improved method for accurate and efficient quantification of MRS data with use of prior knowledge. *J Magn Reson*. 1997;129(1):35-43. doi:10.1006/jmre.1997.1244
45. Chong DGQ, Kreis R, Bolliger CS, Boesch C, Slotboom J. Two-dimensional linear-combination model fitting of magnetic resonance spectra to define the macromolecule baseline using FiTAID, a Fitting Tool for Arrays of Interrelated Datasets. *Magn Reson Mater Phys Biol Med*. 2011;24(3):147-164. doi:10.1007/s10334-011-0246-y
46. Soares AF, Lei H, Gruetter R. Characterization of hepatic fatty acids in mice with reduced liver fat by ultra-short echo time 1H-MRS at 14.1 T in vivo. *NMR Biomed*. 2015;28(8):1009-1020. doi:10.1002/nbm.3345
47. Buehler T, Bally L, Dokumaci AS, Stettler C, Boesch C. Methodological and physiological test–retest reliability of 13C-MRS glycogen measurements in liver and in skeletal muscle of patients with type 1 diabetes and matched healthy controls. *NMR Biomed*. 2016;29(6):796-805. doi:10.1002/nbm.3531
48. Lin A, Andronesi O, Bogner W, et al. Minimum Reporting Standards for in vivo Magnetic Resonance Spectroscopy (MRSinMRS): Experts' consensus recommendations. *NMR in Biomedicine*. 2021;34:e4484. https://doi.org/10.1002/nbm.4484
49. Fillmer A, Hock A, Cameron D, Henning A. Non-water-suppressed 1H MR spectroscopy with orientational prior knowledge shows potential for separating intra- and extramyocellular lipid signals in human myocardium. *Sci Rep*. 2017;7(1):16898. doi:10.1038/s41598-017-16318-0
50. Hock A, MacMillan EL, Fuchs A, et al. Non-water-suppressed proton MR spectroscopy improves spectral quality in the human spinal cord. *Magn Reson Med*. 2013;69(5):1253-1260. doi:10.1002/mrm.24387
51. Pasanta D, Tungjai M, Chancharunee S, Sajomsang W, Kothan S. Body mass index and its effects on liver fat content in overweight and obese young adults by proton magnetic resonance spectroscopy technique. *World J Hepatol*. 2018;10(12):924-933. doi:10.4254/wjh.v10.i12.924
52. Boss A, Ayse SD, Tania B, Roland K, Chris B. Comprehensive spectroscopic investigation of liver metabolism—a feasibility study. In: *Proc Int Soc Magn Reson Med*. Vol.21; 2013:4031.
53. Tkáč I, Deelchand D, Dreher W, et al. Water and lipid suppression techniques for advanced 1H MRS and MRSI of the human brain: experts' consensus recommendations. *NMR Biomed*. 2021;34(5):e4459. doi:10.1002/nbm.4459
54. Pfyffer D, Zimmermann S, Şimşek K, Kreis R, Freund P, Seif M. Magnetic resonance spectroscopy investigation in the right human hippocampus following spinal cord injury. *Front Neurol*. 2023;14:1120227. doi:10.3389/fneur.2023.1120227
55. Gursan A, Hendriks AD, Welting D, de Jong PA, Klomp DWJ, Prompers JJ. Deuterium body array for the simultaneous measurement of hepatic and renal glucose metabolism and gastric emptying with dynamic 3D deuterium metabolic imaging at 7 T. *NMR Biomed*. 2023;36:e4926. doi:10.1002/nbm.4926
56. Nam KM, Gursan A, Bhogal AA, et al. Deuterium echo-planar spectroscopic imaging (EPSI) in the human liver in vivo at 7 T. *Magn Reson Med*. 2022;90(3):863-874. doi:10.1002/mrm.29696
57. Poli S, Emara AF, Ballabani E, et al. DMI using different doses of [6,6′-2H2]-glucose for real-time in vivo liver glucose mapping at 7 T. In: *Proceedings of the 32nd Annual Meeting of the International Society for Magnetic Resonance in Medicine*. #012; 2023.
58. Francischello R, Geppi M, Flori A, Vasini EM, Sykora S, Menichetti L. Application of low-rank approximation using truncated singular value decomposition for noise reduction in hyperpolarized 13 C NMR spectroscopy. *NMR Biomed*. 2021;34(5):e4285. doi:10.1002/nbm.4285

59. Vaziri S, Autry AW, Lafontaine M, et al. Assessment of higher-order singular value decomposition denoising methods on dynamic hyperpolarized [1-13C]pyruvate MRI data from patients with glioma. *NeuroImage Clin*. 2022;36:103155.
60. Liu Y, De Feyter HM, Fulbright RK, McIntyre S, Nixon TW, de Graaf RA. Interleaved fluid-attenuated inversion recovery (FLAIR) MRI and deuterium metabolic imaging (DMI) on human brain in vivo. *Magn Reson Med*. 2022;88(1):28-37. doi:10.1002/mrm.29196

SUPPORTING INFORMATION

Additional supporting information can be found online in the Supporting Information section at the end of this article.

How to cite this article: Poli S, Emara AF, Lange NF, et al. Interleaved trinuclear MRS for single-session investigation of carbohydrate and lipid metabolism in human liver at 7T. *NMR in Biomedicine*. 2024;e5123. doi:10.1002/nbm.5123